STRUCTURE AND BONDING IN HYDROUS MINERALS AT HIGH PRESSURE: RAMAN SPECTROSCOPY OF ALKALINE EARTH HYDROXIDES

T. S. Duffy, R. J. Hemley, and H. K. Mao

Geophysical Laboratory and Center for High-Pressure Research, Carnegie Institution of Washington, 5251 Broad Branch Rd, NW, Washington, DC 20015

ABSTRACT

The high-pressure behavior of the hydrous minerals brucite and portlandite was examined by Raman spectroscopy in a diamond anvil cell. Both the hydrogenated and deuterated forms of brucite [$Mg(OH)_2$, $Mg(OD)_2$] show evidence for structural changes that are first detectable at 4-5 GPa, and these materials remain crystalline to pressures upwards of 30 GPa. Portlandite [$Ca(OH)_2$] becomes amorphous when compressed above 12 GPa. It is proposed that both the structural changes in brucite and amorphization of portlandite are driven by a destabilization of the H substructure as the materials are compressed. In brucite, the hydrogen and deuterium atoms adopt new positions which stabilize the structure to very high pressure. In portlandite, disordering of the hydrogens triggers destabilization of the oxygen substructure, leading to pressure-induced amorphization.

INTRODUCTION

The existence and distribution of volatile species in terrestrial planetary interiors may strongly influence some of the most important physical properties of these bodies, including their viscosity, elasticity, and mineralogy. Hydrogen is particularly significant in this regard, and the possible existence of deep hydrogen reservoirs in the Earth has generated considerable recent interest[1–3]. Little is known, however, about the crystal chemistry and stability of hydrogen-bearing minerals at high pressures and temperatures. In this study, we examine the effects of changes in pressure and chemistry on the behavior of hydrous minerals.

The alkaline earth hydroxides are among the simplest hydrogen-bearing materials, and therefore are useful as prototypes for understanding the role of hydrogen in crystal structures at high pressure. The isostructural hydroxides, brucite, $Mg(OH)_2$, and portlandite, $Ca(OH)_2$, have been the subject of extensive experimental investigation[4–14]. The structural and chemical simplicity of these materials makes them far more amenable to study than the more complex hydrous silicates that have been identified thus far[3]. At the same time, they posses features in common with the more complex phases, including similarities in topology and bonding environments. The crystal structure of brucite and portlandite is shown in Fig. 1.

X-ray diffraction studies[4–7] of these materials have revealed considerable differences in their high-pressure behavior: brucite remains crystalline to 78 GPa at 600 K[4], while portlandite becomes x-ray amorphous when compressed above 12 GPa at room temperature[6] and transforms to a new crystalline structure at pressures as low as 5.6 GPa and 773 K[7]. There are also differences in the infrared spectra of the two materials at high pressure and ambient temperature that are consistent with

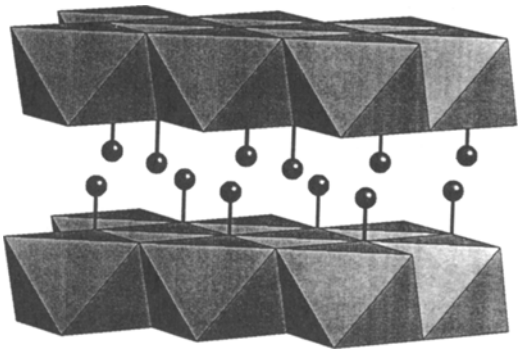

Fig. 1. Crystal structure of brucite and portlandite. Mg/Ca atoms lie at centers of octahedra. Spheres represent hydrogen/deuterium atoms. The hydroxyl bonds are along the *c* axis.

the x-ray results[8]. Neutron diffraction studies of normal and deuterated brucite to 10 GPa provide evidence for H and D disorder at high pressure[9–10] . We have recently reported measurements of the Raman spectra of brucite to 37 GPa, which document a previously undetected phase transition[11]. In this study, we combine this data with new measurements on portlandite and deuterated brucite to probe how chemical changes affect high-pressure behavior within this system.

EXPERIMENTAL TECHNIQUE

Deuterated brucite was supplied by K. Leinenweber from the same material used in their high-pressure neutron diffraction study[9]. Portlandite samples (>95% purity) were purchased commercially (Aldrich Chemical Co.). The latter were contaminated with a small amount of $Ca(CO)_3$ due to reaction with CO_2 in the atmosphere. Fine-grained samples were loaded into a Mao-Bell diamond anvil cell having 600-μm culets. Raman spectra were excited using an Ar^+ laser operated at 488.0 or 514.5 nm and were recorded using a Dilor XY spectrometer equipped with a CCD detector. Experiments on $Mg(OD)_2$ and $Ca(OH)_2$ were conducted under non-hydrostatic conditions (no pressure medium). Spectra of $Mg(OH)_2$ were recorded both non-hydrostatically and under quasi-hydrostatic conditions using neon as a pressure transmitting medium. The Raman spectra are not strongly affected by degree of hydrostaticity[11]. Pressures were determined from the shift of the fluorescence wavelength of small ruby crystals distributed through the sample volume. Further experimental details can be found in Ref. 11.

RESULTS

Factor group analysis indicates there are four Raman-active modes for brucite and portlandite. Three of these are low-frequency lattice vibrations (external modes) and one is a symmetric OH-stretch vibration (internal mode). Ambient-pressure Raman spectra for $Mg(OH)_2$, $Mg(OD)_2$, and $Ca(OH)_2$ in the low-frequency region are shown in Figure 2a. The ambient-pressure OH-stretch vibrations of $Mg(OH)_2$ and $Ca(OH)_2$ are shown in Figure 2b. For each material, all the expected modes are observed, and agreement with previous data[12] is excellent.

For the translational modes, E_g(T) and A_{1g}(T), there are only small shifts in frequency between the protonated and deuterated forms of brucite. The E_g(T) mode of portlandite is of very low intensity relative to brucite. The librational

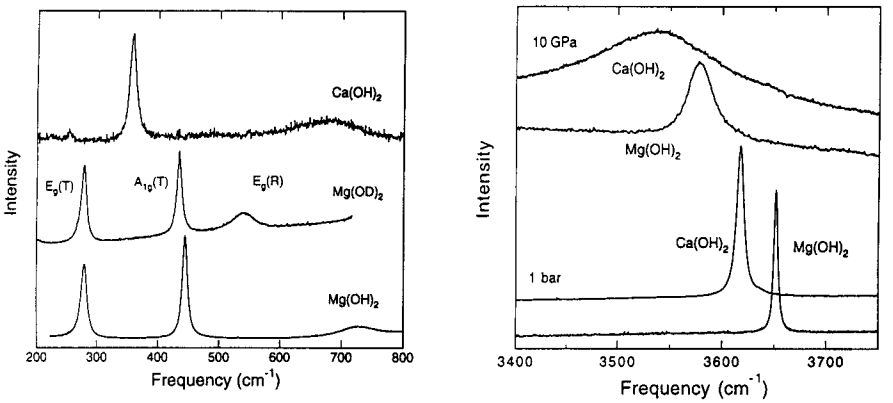

Fig. 2. (a) Ambient-pressure external Raman modes of $Ca(OH)_2$, $Mg(OD)_2$, and $Mg(OH)_2$. E_g (T) and A_{1g} (T) are translational vibrations of the OH or OD groups perpendicular and parallel to the c axis, respectively. The broad E_g (R) mode is a librational motion of the OH or OD unit. (b) OH-stretch modes of brucite and portlandite at ambient pressure and at 10 GPa under non-hydrostatic compression.

modes, E_g(R), are broad and weak for all three materials. In general, the linewidths of all vibrational modes of $Ca(OH)_2$ are about a factor of two larger than those in either form of brucite. This may be consistent with evidence from neutron diffraction for dynamic H disorder in $Ca(OH)_2$ at ambient pressure[13] or it may reflect differences in grain size.

Figure 3 shows the behavior of the external and internal vibrational modes of deuterated brucite under non-hydrostatic compression to pressures of 30 GPa and 24 GPa, respectively. In general, the $Mg(OD)_2$ results are very similar to earlier $Mg(OH)_2$ data[11]. At 5 GPa, a new line is first detectable between the E_g and A_{1g} modes (Fig. 3a). This line subsequently grows at the expense of the E_g mode over a broad pressure interval, with the intensity ratio of the peaks varying approximately exponentially with pressure. The two peaks approach each other and reach a minimum in frequency separation at about 24 GPa (Fig. 4a). These features are characteristic of a Fermi resonance in which two modes of the same symmetry are coupled by an interaction term in the Hamiltonian. The development of the resonance in $Mg(OD)_2$ is similar to the resonance previously observed in $Mg(OH)_2$[11]. The lack of a significant isotope effect is not surprising as the translational modes are not strongly affected by substitution of D for H. The coupling coefficient, estimated by one-half the minimum frequency separation, is $\sim$11 cm^{-1} for $Mg(OD)_2$, compared to $\sim$9 cm^{-1} for $Mg(OH)_2$.

The high-pressure behavior of the internal mode in deuterated brucite is also similar to $Mg(OH)_2$ (Fig. 3b). In contrast to the external modes, the OH-stretch and OD-stretch vibrations decrease in frequency with increasing pressure. Such behavior is normally associated with hydrogen bonding[8]. A high-frequency sideband on the primary OD stretch is first detected at 5 GPa, consistent with previous detection of a sideband on the OH mode of $Mg(OH)_2$[11] at 4 GPa. Between 14

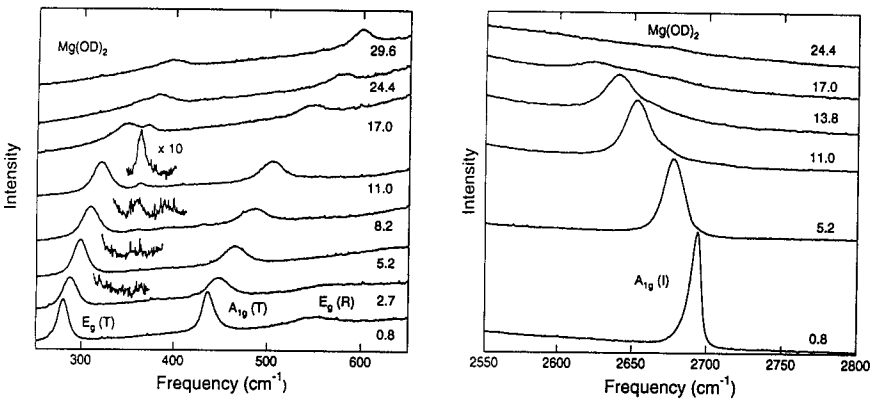

Fig. 3. (a) External modes of $Mg(OD)_2$ under non-hydrostatic compression The pressure (in GPa) is shown next to each trace. An expanded view of the high-frequency side of the E_g (T) mode is shown between 2.7 and 11.0 GPa. (b) OD-stretch vibration of deuterated brucite under non-hydrostatic compression to 24 GPa. A high-frequency sideband is visible at pressures of 5.2 GPa and above.

and 17 GPa, the OD stretch vibration weakens and broadens considerably, and the peak cannot be detected above this pressure. The weakening and disappearance of the symmetric stretch is also observed in $Mg(OH)_2$, but at higher pressures (20-28 GPa).

In general, the substitution of D for H has only minor effects on the high-pressure behavior of the vibrational modes of brucite. New Raman lines are detected in deuterated brucite around 5 GPa, near the pressure (4 GPa) at which similar features were detected in $Mg(OH)_2$. Both materials exhibit a Fermi resonance over a comparable pressure range. The pressure dependence of the vibrational frequencies of $Mg(OH)_2$ and $Mg(OD)_2$ are shown in Figure 4 and Table I.

The vibration modes of $Ca(OH)_2$ were measured to 14 GPa under non-hydrostatic conditions (Fig. 4). No evidence for a crystalline phase transition was found over this range. The E_g(T) mode is difficult to detect in this material, but the E_g(R) mode can be observed at elevated pressures. As with brucite, the OH-vibration decreases in frequency with pressure, but this decrease becomes non-linear above about 5 GPa. The width of the OH-stretching vibration begins to increase strongly above this pressure as well (Fig. 5). At 10.4 GPa, the linewidth of the OH-stretch vibration in portlandite is almost an order of magnitude larger than in brucite (Fig. 2b). Between 10.4 and 12.5 GPa, the amplitude of the OH-stretch vibration decreases dramatically (Fig. 6). Over this same range, the only observable lattice vibration (A_{1g}) similarly becomes weak and broad. This is the same pressure range over which portlandite becomes x-ray amorphous[6], and comparable peak broadening is observed for the infrared-active OH-stretch vibration[8] at these pressures. Upon decompression from 14 GPa, the Raman peaks remain very weak and broad until near 2 GPa, at which point they abruptly recover.

DISCUSSION

The new Raman data for brucite and portlandite complement other recent data[4–14] for these materials and allows for a better understanding of their structural response to compression. In the case of brucite, substitution of D for H produces only relatively minor changes in ambient-pressure structural parameters (Table II). The Raman spectra of $Mg(OH)_2$ and $Mg(OD)_2$ are also similar at high pressures (Figs. 3 and 4), with new peaks appearing in the spectrum of both materials at 4-5 GPa. Due to their weak initial intensity, determination of the pressure at which these peaks first appear is difficult and limited by spectral quality. At ambient pressure, there is no evidence for additional peaks in high-quality spectra for both $Mg(OH)_2$ and $Mg(OD)_2$ (Fig. 2). Therefore, we believe that observed features are due to a phase transition at high pressure rather than due to intensity enhancement of peaks present at ambient pressure.

Table I. Pressure dependence of Raman modes.

		$\nu = A + BP + CP^2$			
Mode	Obs. P range (GPa)	A (cm^{-1})	B (cm^{-1}/GPa)	C (cm^{-1}/GPa^2)	γ_{i0}[a]
		$Mg(OH)_2$			
E_g(T)	0-37	280.0	5.40	-0.08	0.81
	4-37	359.6	0.60	0.02	
A_{1g}(T)	0-37	444.7	6.93	-0.08	0.65
E_g(R)	0	727.5			
A_{1g}(I)	0-28	3652.0	-7.68		-0.09
	4-20	3661.3	-5.34		
		$Mg(OD)_2$			
E_g(T)	0-30	278.5	4.26	-0.04	0.64
	5-30	346.2	1.30	0.01	
A_{1g}(T)	0-30	434.8	6.48	-0.03	0.63
E_g(R)	0-3	537.5	11.69		0.91
A_{1g}(I)	0-17	2694.4	-4.01		-0.06
	5-17	2709.9	-3.25		
		$Ca(OH)_2$			
E_g(T)	0-9	253.5	5.68	0.07	0.85
A_{1g}(T)	0-12	356.8	8.78	-0.25	0.94
E_g(R)	0-12	671.5	21.34	-1.15	1.21
A_{1g}(I)	0-12	3617.5	-3.68	-0.41	-0.04

[a]Ambient pressure mode Grüneisen parameters computed using a bulk modulus of 42 GPa for brucite and 38 GPa for portlandite.

Neutron diffraction data[9] for $Mg(OD)_2$ are consistent with a structural change at 5.4 GPa. Improved fits to the neutron data are obtained at this pressure by allowing the D atoms to be split over three off-axis sites. Such a model is consistent with the Raman spectra for $Mg(OD)_2$, which were obtained on the same

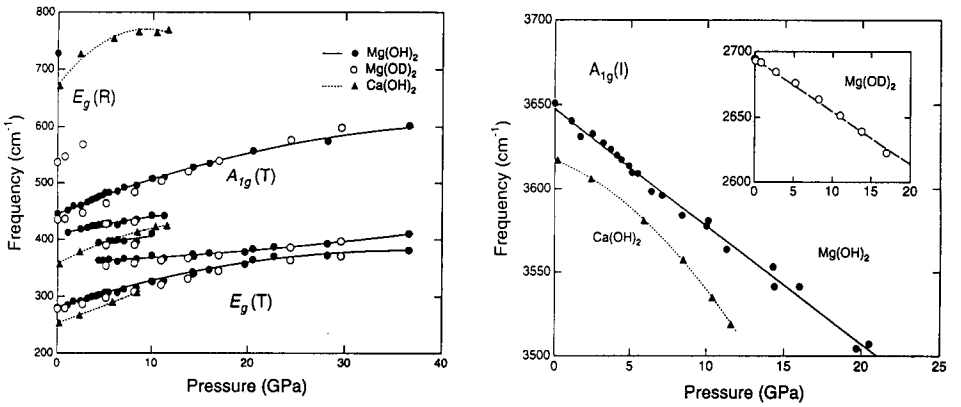

Fig. 4. (a) Pressure-dependence of Raman frequencies for $Ca(OH)_2$, $Mg(OH)_2$, and $Mg(OD)_2$. Lines show fits to data for $Ca(OH)_2$ and $Mg(OH)_2$, but fits are omitted for $Mg(OD)_2$ for clarity. (b) Pressure-dependence of OH/OD-stretch vibrational frequencies.

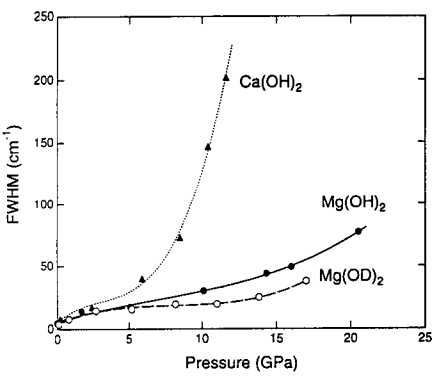

Fig. 5. Band width of the OH-stretch vibrations under non-hydrostatic compression. FWHM is full width at half maximum.

sample material as used in the neutron study. The neutron data[10] for $Mg(OH)_2$ is also consistent with H disordering, but only at a higher pressure of 10.9 GPa. Neutron studies of the two materials also yield different results for the pressure dependence of the O-H and O-D bond lengths. For $Mg(OD)_2$, a slight lengthening of the O-D distance with pressure is reported, whereas for $Mg(OH)_2$ the O-H bond length remains nearly constant or contracts slightly with pressure. One possible interpretation of the neutron results is that disordering occurs more easily and interlayer bonding becomes stronger with pressure in the deuterated form of brucite. However, our Raman measurements indicate that the two materials behave similarly, and that structural changes occur at nearly the same pressure in both forms of brucite. Hence, it is probable that the apparent differences between the two neutron studies arise from differences in experimental technique or data analysis, rather than from intrinsic differences in the high-pressure response of $Mg(OH)_2$ and $Mg(OD)_2$.

All three materials show strong negative frequency shifts (-4 to -8 cm^{-1}/GPa)

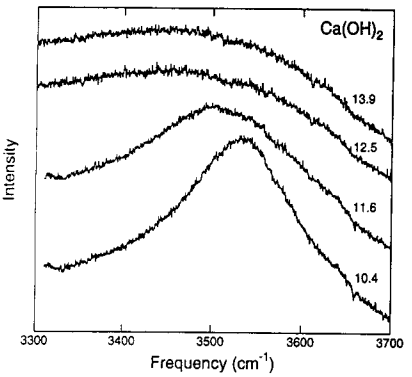

Fig. 6. OH-stretch vibration in portlandite between 10.4 and 13.9 GPa. The strong reduction in peak intensity over a narrow pressure interval is evident. Pressures are listed in GPa next to each trace.

of the Raman-active OH-stretch with pressure (Fig. 4b). The underlying cause of this red-shift of the internal mode frequencies with pressure is unclear from currently available data. It is generally assumed that such behavior arises from decreasing force constants and concomitant lengthening of the O-H/O-D bond as a consequence of increased hydrogen bonding[8]. However, it is important to note that a decreasing force constant does not require bond expansion[15] (i.e., the length could remain unchanged or could even compress).

The ratio of the Raman-active stretch frequencies in $Mg(OH)_2$ and $Mg(OD)_2$ is 1.355 at ambient pressure, and decreases weakly with pressure to 1.341 at 18 GPa. The expected ratio (for a purely harmonic interaction) given by the ratio of reduced masses is 1.376. This indicates there is some anharmonicity which increases slightly with pressure. The lower than expected frequency ratio and its decrease with pressure has been observed in some molecular crystals[16].

A comparison of the behavior of brucite and portlandite at high pressure may yield insights into the process of pressure-induced amorphization. There are a number of differences between our results for $Ca(OH)_2$ and earlier high-pressure Raman data for this material[14], which were obtained with a less sensitive detector (diode array). We have detected all the Raman active modes of portlandite at ambient pressure (Table I) and our results are in good agreement with earlier work[12] that assigned modes on the basis of polarized spectra and deuterated samples. We therefore assign the strong mode at 356.8 cm^{-1} to be the A_{1g} (T) mode rather than the E_g (T) mode as was done previously[14]. Ref. 14 also reports the appearance of new modes near 3650 cm^{-1} at 11 GPa, and near 750 cm^{-1} at 13 GPa. We find no evidence for a new mode near 3650 cm^{-1} up to 14 GPa (Fig. 6). Furthermore, the mode near 750 cm^{-1} may be the E_g (R) mode that we detect near this frequency up to 11.6 GPa (Fig. 4a). Thus, in contrast to Ref. 14, we find no evidence for the appearance of new Raman lines in this material at high pressure. Above 11.6 GPa, we find evidence for only very broad and weak Raman peaks in portlandite, consistent with infrared data[8]. The pressure dependences of the A_{1g} internal and external mode frequencies determined in this study are the same as those found previously[14].

The high-pressure response of $Ca(OH)_2$ can be divided into three regions on

the basis of Raman measurements. At low pressures (to 5 GPa) portlandite behaves in a manner analogous to $Mg(OH)_2$ over than same pressure range. From 5-12 GPa, qualitative changes in the Raman spectra are observed. Specifically, the OH-stretch frequency in $Ca(OH)_2$ begins to decrease non-linearly with pressure (Fig. 4b) and its band width increases significantly relative to the band width of the brucite peak (Fig. 5). At about 12 GPa, all portlandite peaks abruptly weaken and merge with the background (Fig. 6). Both IR and x-ray diffraction peaks disappear at a similar pressure, implying that disordering occurs at both spectroscopic and x-ray length scales. It has been suggested that pressure-induced amorphization in portlandite is due to a kinetically inhibited phase transition. A phase transition in $Ca(OH)_2$ has been observed at 5.6 GPa and 773 K[7]. While pressure-induced amorphization occurs at much higher pressure than this, the Raman data provide evidence that structural changes begin to occur near this pressure.

Table II. Ambient-pressure structural parameters.

	$Mg(OH)_2$[a]	$Mg(OD)_2$[b]	$Ca(OH)_2$[c]
a (Å)	3.14979(4)	3.1455(1)	3.5918(3)
c (Å)	4.7702(1)	4.7646(3)	4.9063(7)
c/a	1.51445(4)	1.5147(1)	1.3659(2)
V (Å^3)	40.986(1)	40.831(4)	54.816(12)
ρ (g/cm^3)	2.362	2.453	2.244
z_0	0.2203(3)	0.2218(3)	0.2341(3)
z_H/z_D	0.4130(6)	0.4183(2)	0.4248(6)
Mg-O/Ca-O (Å)	2.1003(6)	2.1012(6)	2.371(1)
O-H/O-D (Å)	0.958(3)	0.956	0.984(4)
H...H′/D...D′ (Å)	1.999(2)	1.960	2.202(2)
O...O′ (Å)	3.229(2)	3.2133(1)	3.333(2)

[a]Ref. 10, [b]Ref. 17, [c]Ref. 18 (see also Ref. 13).

The three hydroxide compositions examined here provide evidence for a range of high-pressure behavior even within this simple structure. Recently, pressure-induced amorphization has been observed at 11.2 GPa by IR spectroscopy in the isomorphous transition metal hydroxide, $Co(OH)_2$, with evidence for structural changes continuing in the amorphous state to 36 GPa[19]. In brucite, modifications to the H substructure appear to be sufficient to allow the oxygen substructure to remain intact to very high pressures. In portlandite, on the other hand, complete disordering of both the O and H substructure occur at similar pressures. This collapse is preceded by a pressure range over which there is evidence for precursory disordering within the H substructure alone. This disordering begins near the pressure where the H substructure of brucite rearranges itself and where a crystalline phase transition has been observed in portlandite at elevated temperature.

In summary, Raman spectroscopic data for portlandite, and both hydrogenated and deuterated forms of brucite can be interpreted with a simple model that describes the differences in their high-pressure behavior. At low pressures, the H

atoms begin to be displaced from their equilibrium positions in these materials due to increased interlayer forces as the structure is compressed. In the case of brucite, the H atoms adopt new positions, possibly in a three-site disordered arrangement, which stabilizes the structure to high pressures. In portlandite, broadening of the Raman peaks between 5 and 12 GPa indicates that the H atoms become increasingly disordered over this range, leading to a range of bond distances, orientations, and strengths. The larger intralayer O-O distances in $Ca(OH)_2$ may prevent the H atoms from achieving stable positions. The disorder in the H substructure triggers disordering of the O sublattice at about 12 GPa. This leads to destabilization of the structure as a whole and relatively extensive amorphization over a narrow pressure interval in this material.

Despite being among the simplest hydrogen-bearing minerals, the alkaline earth hydroxides exhibit complex and varied responses to the application of pressure. Characterization of this behavior requires the use of a variety of in situ experimental probes (spectroscopy, neutron and x-ray diffraction). Such detailed analyses are necessary to achieve an understanding of the crystal chemistry of hydrogen-bearing minerals under Earth mantle conditions.

ACKNOWLEDGEMENTS

K. Leinenweber provided samples of $Mg(OD)_2$. We benefited from discussions and correspondence with Q. Williams, J. Parise, K. Leinenweber, M. Catti, and C. Meade. R. Downs is thanked for technical assistance. This work was supported by the NSF.

REFERENCES

1. A. B. Thompson, Nature **358**, 295 (1992).
2. M. Kanzaki, Phys. Earth Planet. Int. **66**, 307 (1991).
3. L. W. Finger and C. T. Prewitt, Geophys. Res. Lett. **16**, 1395 (1989).
4. Y. Fei and H. K. Mao, J. Geophys. Res. **98**, 11875 (1993).
5. T. S. Duffy, J. Shu, H. K. Mao, and R. J. Hemley, Phys. Chem. Minerals, in press.
6. C. Meade and R. Jeanloz, Geophys. Res. Lett. **17**, 1157 (1990).
7. K. Leinenweber, *Natl. Synchrotron Light Source Activity Rep.* (Brookhaven National Laboratory, Upton, NY, 1993) p. 128; M. Kunz, D. J. Weidner, J. B. Parise, M. Vaughan, and Y. Wang, Eos Trans. AGU, Fall Meeting Suppl., 661 (1994).
8. M. B. Kruger, Q. Williams, and R. Jeanloz, J. Chem. Phys. **91**, 5910 (1989).
9. J. B. Parise, K. Leinenweber, D. J. Weidner, K. Tan, and R. B. Von Dreele, Am. Mineral. **79**, 193 (1994).
10. M. Catti, G. Ferraris, S. Hull, and A. Pavese, Phys. Chem. Minerals, in press.
11. T. S. Duffy, C. Meade, Y. Fei, R. J. Hemley, and H. K. Mao, Am. Mineral. **80**, 222 (1995).
12. P. Dawson, C. D. Hadfield, and G. R. Wilkinson, J. Phys. Chem. Solids **34**, 1217 (1973).
13. L. Desgranges, D. Grebille, G. Calvarin, G. Chevrier, N. Floquet, and J. C. Niepce, Acta Cryst. **B49**, 812 (1993).

14. C. Meade, R. Jeanloz, and R. J. Hemley, in *High-Pressure Research: Applications to Earth and Planetary Science* (Terra Scientific, Tokyo, 1992), p. 485.
15. R. J. Nelmes et al., Phys. Rev. Lett. **71**, 1192 (1993).
16. H. Shimizu, Phys. Rev. **B32**, 4120 (1985).
17. D. E. Partin, M. O'Keefe, and R. B. Von Dreele, J. Appl. Cryst. **27**, 581 (1994).
18. W. R. Busing and H. A. Levy, J. Chem. Phys. **26**, 563 (1957).
19. J. H. Nguyen, M. B. Kruger, and R. Jeanloz, Phys. Rev. B **49**, 3734 (1994).